Further Study on Robust Adaptive Beamforming With Optimum Diagonal Loading

Ayman Elnashar, Said M. Elnoubi, and Hamdi A. El-Mikati, *Senior Member, IEEE*

***Abstract*—Significant effort has gone into designing robust adaptive beamforming algorithms to improve robustness against uncertainties in array manifold. These uncertainties may be caused by uncertainty in direction-of-arrival (DOA), imperfect array calibration, near-far effect, mutual coupling, and other mismatch and modeling errors. A diagonal loading technique is obligatory to fulfill the uncertainty constraint where the diagonal loading level is amended to satisfy the constrained value. The major drawback of diagonal loading techniques is that it is not clear how to get the optimum value of diagonal loading level based on the recognized level of uncertainty constraint. In this paper, an alternative realization of the robust adaptive linearly constrained minimum variance beamforming with ellipsoidal uncertainty constraint on the steering vector is developed. The diagonal loading technique is integrated into the adaptive update schemes by means of optimum variable loading technique which provides loading-on-demand mechanism rather than fixed, continuous or *ad hoc* loading. We additionally enrich the proposed robust adaptive beamformers by imposing a cooperative quadratic constraint on the weight vector norm to overcome noise enhancement at low SNR. Several numerical simulations with DOA mismatch, moving jamming, and mutual coupling are carried out to explore the performance of the proposed schemes and compare their performance with other traditional and robust beamformers.**

***Index Terms*—Adaptive beamforming, Capon beamformer, conjugate gradient, constrained optimization, diagonal loading, linearly constrained minimum variance (LCMV) beamforming, moving jamming, mutual coupling, steepest descent.**

I. Introduction

ADAPTIVE beamforming has been exploited in wireless communications, radar, sonar, speech processing, and other areas. Recently, there has been a great effort to design robust adaptive beamforming techniques which improve robustness against mismatch and modeling errors and enhancing interference cancellation capability. There are several existing approaches to robust adaptive beamforming. The so-called linearly constrained minimum variance (LCMV) beamformer, also known as Capon's method, has been a popular beamforming technique [1]–[3]. In LCMV beamforming method, the weights are chosen to minimize the array output power subject to side constraint(s) in the desired look direction(s). This method assumes that the array manifold is accurately known, unfortunately, even small discrepancy between the presumed and the actual array manifold can substantially degrade its performance [4].

Diagonal loading technique has been a widespread approach to improve robustness against mismatch errors, random perturbations, and small sample support [5]–[8]. Furthermore, it is well-known that antenna sidelobes can be made small if the sample data covariance matrix is diagonally loaded before inversion is performed. The main drawback of the diagonal loading techniques is the difficulty to derive a closed-form expression for the diagonal loading term which relates the amount of diagonal loading with the upper bound of the mismatch uncertainty or the required level of robustness. In addition, small interference signals should not be masked below loading level because the adaptive system will de-emphasize their importance relative to added signal [6]. The asymptotic analysis provided in [7] establishes the existence of an optimum loading factor, which can be estimated from the received data.

Recently, variable loading (VL) techniques for implementing a quadratic inequality constraint on the beamformer weights to improve robustness against pointing errors and random perturbations in detector parameters are proposed in [8] and [9]. In these approaches multiple constraints are imposed during output power minimization to preserve several desired directions (users) while the quadratic constraint is applied on the weight vector in preference to the steering or signature vectors. Therefore, these approaches can be interpreted as general robust techniques where the constrained value is not explicitly related to the uncertainties in the steering vectors.

Very recently, robust beamforming approaches are developed in [10]–[13] and derived from the standard single constraint LCMV beamforming with a spherical or ellipsoidal uncertainty constraint. The uncertainty constraint is imposed directly on the steering vector. The approach proposed in [12] reformulates the robust adaptive beamforming as a convex second order cone programming (SOCP). The SOCP approach can be interpreted as a diagonal loading technique in which the optimal value of diagonal loading is computed based on the known upper bound on the norm of the signal steering vector mismatch [12]. The SeDuMe optimization Matlab toolbox [14] can be used to compute the weight vector of SOCP approach. Unfortunately, the computational burden of this software seems to be cumbersome which limits the practical implementation of this technique. In addition to this and although several efficient convex optimization software tools are currently accessible, the SOCP-based method

Manuscript received February 9, 2005 ; revised August 17, 2006.

A. Elnashar is with the Department of Mobile Network Development (MND), Etihad Etisalat (mobily), Riyadh 11423, Saudi Arabia (e-mail: a.elnashar@mobily.com.sa or anashar@gmail.com).

S. M. Elnoubi is with the Department of Electrical Engineering, Alexandria University, Alexandria 21544, Egypt, (e-mail: selnoubi@hotmail.com).

H. A. El-Mikati is with the Department of Electronic Engineering, Mansoura University, Mansoura 35516, Egypt (e-mail: h.elmikati@ieee.org).

Color version of Fig. 6 is available online at http://ieeexplore.ieee.org.

Digital Object Identifier 10.1109/TAP.2006.886473

does not provide any closed-from solution, and does not have simple on-line implementation [15]. Therefore, this technique is considered as batch algorithm rather than recursive scheme where the weight vector of this beamformer is independently computed in each step and can not be updated recursively.

The robust Capon beamformer proposed in [13] precisely computes the diagonal loading level based on *ellipsoidal uncertainty* set of array steering vector. The essence behind this technique is the estimation of signal of interest power (SOIP) rather than the signal itself. An eigendecomposition batch algorithm is proposed to compute the diagonal loading level which would also hit the wall of computational complexity. Alternatively, this approach can be recursively implemented using subspace tracking algorithms via tracking signal and noise subspaces. However, it is difficult to apply this approach to wireless communications where the dimension of signal and noise may be ambiguous or not exactly known. Besides, the eigendecomposition approach is based on *continuous* diagonal loading even without mismatch [10], [11]. Specifically, the data covariance matrix will be diagonally loaded even without mismatch errors as in desired source moving scenario.

The contribution of this paper is two-fold. We first develop a recursive realization for the robust LCMV beamforming which includes uncertainty ellipsoidal constraint on the steering vector (see, also, [10] and [11]). The robust recursive implementation presented here is based on combination of the ellipsoidal constraint formulation provided in [13] with a reformulation of the VL technique provided in [9]. As a consequence, an accurate technique for computing the diagonal loading level without eigendecomposition or SOCP is presented. The diagonal loading technique is integrated into the recursive algorithm using loading-on-demand mechanism. The geometrical interpretation of the proposed diagonal loading technique is illustrated to compare it with eigendecomposition approach. The second contribution of this work is the development of a joint constraint approach for a joint robustness beamformer. A joint constraint approach is presented in [16] for joint robustness against steering vector mismatch and unstationarity of interferers. We alternatively impose an ellipsoidal uncertainty constraint and a quadratic constraint on the steering vector and the beamformer weights, respectively. We take the cue of the quadratic constraint solution from [5] and [8]. We additionally propose a new simple approach to get the corresponding diagonal loading value. The quadratic constraint is invoked as a cooperative constraint to overcome noise enhancement at low SNR. In addition, it is demonstrated in [17] that the peak sidelobe level of the adaptive patterns can be controlled to the desired level by constraining the perturbation of the adaptive weights to the quiescent weight vector.

The rest of the paper is organized as follows. In Section II, a generalized antenna array model with mutual coupling and the standard LCMV beamforming approach are summarized. In Section III, the formulation of robust beamforming, diagonal loading approach, joint constraint methodology, improved recursive implementation, and geometric interpretation are presented. Computer simulations and performance comparison are provided in Section IV. Conclusions and points for future work are summarized in Section V.

II. Background

Consider a linear array with M sensors. The array received signal $\boldsymbol{x}(n)$ is $M\times\ 1$ vector and can be written as [18]

$$\boldsymbol{x}(k)=\sum_{i=0}^{L-1}\boldsymbol{C}\boldsymbol{a}_i(\theta_i)\boldsymbol{s}_i(k)+\boldsymbol{v}(k) \tag{1}$$

where $\boldsymbol{s_i}(k)$ is the k^{th} sample transmitted by i^{th} source, L is the number of sources, $\boldsymbol{a_i}$ is the $M\times\ 1$ complex array steering vector in the direction θ_i, C is $M\times M$ mutual coupling matrix and $\boldsymbol{v}(k)$ is the complex vector of ambient channel noise samples and are assumed to be independent and identically distributed (i.i.d.) random variables with Gaussian distribution, i.e.

$$\boldsymbol{v}(k)\in\left\{N\left(0,\sqrt{\frac{\sigma_v^2}{2}}\boldsymbol{I}_M\right)+iN\left(0,\sqrt{\frac{\sigma_v^2}{2}}\boldsymbol{I}_M\right)\right\} \tag{2}$$

where σ_v^2, i, N, and $\boldsymbol{I}_M$ stand, respectively, for noise power, complex term, Gaussian random generator, and $M\times M$ identity matrix.

Equation (1) can be simplified by defining an effective array steering vector $\boldsymbol{a}_i(\theta_i)=\boldsymbol{C}\boldsymbol{a}_i(\theta_i)$. Array calibration methods attempt to estimate the matrix $\boldsymbol{C}$ off-line or on-line or directly measure the effective array steering vector $\boldsymbol{a}_i(\theta_i)$ using field measurements [19]. The mutual coupling matrix is generally assumed to be independent of DOA. The mutual coupling matrix $\boldsymbol{C}$ (sometimes termed as distortion matrix) can be expressed using the fundamentals of electromagnetic theory as [18]

$$\boldsymbol{C}=(Z_A+Z_T)\left(\boldsymbol{Z}+Z_T\boldsymbol{I}\right)^{-1} \tag{3}$$

where Z_A is the array element's impedance in isolation (for dipole with $\lambda/2$ length, $Z_A=73+j42.5\,[\Omega]$), Z_T is the terminating impedance of the receiver at each antenna element and it is adjusted to the complex conjugate of Z_A for impedance matching, and $\boldsymbol{Z}$ is the mutual impedance matrix. If Z_T is increased, the coupling matrix $\boldsymbol{C}$ converges to the unity matrix and subsequently the effect of mutual coupling is suppressed at the cost of increased impedance mismatch and hence more power loss. The matrix $\boldsymbol{Z}$ can be obtained using method of moments (MoM), or full-wave electromagnetic computation [18], [20]. For dipoles, the matrix $\boldsymbol{Z}$ can be obtained using classical induced electromotive force (EMF) method. In this paper, the mutual impedance matrix is estimated using the Matlab script provided in [20].

The beamformer output $y(k)$ is a linear combination of the array sampled received signals at each sensor, i.e.

$$y(k)=\boldsymbol{w}^H(k)\boldsymbol{x}(k) \tag{4}$$

where $\boldsymbol{w}^H(n)$ is $M\times\ 1$ complex vector consists of beamformer weights and $(\cdot)^H$ stands for the Hermitian transpose. The beamformer output energy is given by

$$E\left\{\left|\boldsymbol{y}(k)\right|^2\right\}=E\left\{\left|\boldsymbol{w}^H\boldsymbol{x}(k)\right|^2\right\}=\boldsymbol{w}^H\boldsymbol{R}_{xx}(k)\boldsymbol{w} \tag{5}$$

where $\boldsymbol{R}_{xx}(k) = E\left\{\boldsymbol{x}(k)\boldsymbol{x}^H(k)\right\}$ is the data covariance matrix of the array observations signals $\boldsymbol{x}(k)$.

The conventional LCMV beamformer can be obtained by minimizing the output energy of the beamformer subject to certain number of constraints. To preclude the cancellation of desired signal source, a linear constraint of the form $\boldsymbol{w}^H\boldsymbol{a}_0(\theta_0) = 1$ is imposed throughout the optimization (the mutual coupling effect is ignored for the time being), where $\boldsymbol{a}_0$ is the array steering vector and θ_0 is the DOA of the desired source, that is

$$\min_{\boldsymbol{w}} \boldsymbol{w}^H\boldsymbol{R}_{xx}\boldsymbol{w} \quad \text{subject to} \quad \boldsymbol{w}^H\boldsymbol{a}_0(\theta_0) = 1. \tag{6}$$

The well-known LCMV beamformer is the solution to (6) and can be obtained using the Lagrange method

$$\boldsymbol{w}_0 = \frac{\boldsymbol{R}_{xx}^{-1}\boldsymbol{a}_0(\theta_0)}{\boldsymbol{a}_0^H(\theta_0)\boldsymbol{R}_{xx}^{-1}\boldsymbol{a}_0(\theta_0)}. \tag{7}$$

III. Robust Beamforming Design

A. Basic Formulation

A major drawback of the conventional beamforming in (7) is the sensitivity to the mismatch between presumed and genuine steering vector. A robust adaptive beamforming technique is required to improve the robustness of the conventional beamforming against mismatch errors. In [13], a modified formulation is proposed to obtain a robust Capon beamforming with $O\left(M^3\right)$ flops. This robust Capon beamforming can be obtained by maximizing the beamformer output power after the interference has been rejected subject to nondegenerate ellipsoidal uncertainty set. Consequently, the following max/min formulation of the robust Capon beamformer can be obtained as (see [21] and references therein)

$$\max_{\hat{\boldsymbol{a}}_0}\min_{\boldsymbol{w}} \boldsymbol{w}^H\boldsymbol{R}_{xx}\boldsymbol{w} \text{ subject to } \boldsymbol{w}^H\hat{\boldsymbol{a}}_0(\theta_0) = 1; (\hat{\boldsymbol{a}}_0(k) - \overline{\boldsymbol{a}}_0)^H\boldsymbol{H}^{-1}(\hat{\boldsymbol{a}}_0(k) - \overline{\boldsymbol{a}}_0) \le 1. \tag{8}$$

This optimization problem can be simplified without loss of generality by setting $\boldsymbol{H}^{-1} = 1/\varepsilon\boldsymbol{I}_M$ and solving the inner optimization problem by injecting the standard robust Capon beamformer (7) into (8), which yields

$$\max_{\hat{\boldsymbol{a}}_0} \frac{1}{\hat{\boldsymbol{a}}_0^H(k)\boldsymbol{R}_{xx}^{-1}(k)\hat{\boldsymbol{a}}_0(k)} \text{ subject to } (\hat{\boldsymbol{a}}_0(k) - \overline{\boldsymbol{a}}_0)^H(\hat{\boldsymbol{a}}_0(k) - \overline{\boldsymbol{a}}_0) \le \varepsilon \tag{9}$$

where ε is the ellipsoidal constrained value, $\overline{\boldsymbol{a}}_0$ is the presumed steering vector and $\hat{\boldsymbol{a}}_0(k)$ is the estimated (*genuine*) steering vector with mismatch and other errors are encountered. The optimization problem in (9) can be rewritten as

$$\min_{\hat{a}_0} \hat{\boldsymbol{a}}_0^H(k)\boldsymbol{R}_{xx}^{-1}(k)\hat{\boldsymbol{a}}_0(k) \text{ subject to } \left\|\hat{\boldsymbol{a}}_0(k) - \overline{\boldsymbol{a}}_0\right\|^2 \le \varepsilon. \tag{10}$$

Therefore, the ellipsoidal uncertainty set is reduced to spherical constraint. This problem can be solved using the Lagrange method by forming the following cost function:

$$\Psi_{\hat{\boldsymbol{a}}_0}(k) = \hat{\boldsymbol{a}}_0^H(k)\boldsymbol{R}_{xx}^{-1}(k)\hat{\boldsymbol{a}}_0(k) + \frac{\lambda}{2}t\left(\left\|\hat{\boldsymbol{a}}_0(k) - \overline{\boldsymbol{a}}_0\right\|^2 - \varepsilon\right) \tag{11}$$

where $t\,()$ is the step function and Lagrange multiplier λ is a real scalar determined from ε. The problem is converted from constrained minimization to unconstrained minimization problem and the solution is given by [13]

$$\hat{\boldsymbol{a}}_0 = \left(\frac{\boldsymbol{R}_{xx}^{-1}(k)}{\lambda} + \boldsymbol{I}_M\right)^{-1}\overline{\boldsymbol{a}}_0. \tag{12}$$

It is noteworthy that the step function is introduced to guarantee that the term $\left(\left\|\hat{\boldsymbol{a}}_0(k) - \overline{\boldsymbol{a}}_0\right\|^2 - \varepsilon\right)$ is positive term. Therefore, the step function was not differentiated during optimization of (11). Additionally, the diagonal loading term λ should be positive to guarantee that the matrix $\left(\boldsymbol{R}_{xx}^{-1}(k)/\lambda + \boldsymbol{I}_M\right)$ is positive definite. The robust Capon beamformer $\hat{\boldsymbol{w}}_0$ can be obtained by injecting (12) into (7), thus

$$\hat{\boldsymbol{w}}_0 = \frac{\boldsymbol{R}_{xx}^{-1}\hat{\boldsymbol{a}}_0(\theta_0)}{\hat{\boldsymbol{a}}_0^H(\theta_0)\boldsymbol{R}_{xx}^{-1}\hat{\boldsymbol{a}}_0(\theta_0)}. \tag{13}$$

Regrettably, the value of diagonally loading term λ can not be easily predicted where there is no closed-form expression for the optimal loading level. In [13], a *batch* algorithm for solving this problem has been developed by applying the matrix inversion lemma to (12), which yields

$$\hat{\boldsymbol{a}}_0 = \overline{\boldsymbol{a}}_0 - (\boldsymbol{I}_M + \lambda\boldsymbol{R}_{xx})^{-1}\overline{\boldsymbol{a}}_0. \tag{14}$$

Therefore, based on the spherical constraint in (10), the Lagrange multiplier λ can be obtained as the solution to the following equation:

$$g(\lambda) \triangleq \left\|(\boldsymbol{I}_M + \lambda\boldsymbol{R}_{xx})^{-1}\overline{\boldsymbol{a}}_0\right\|^2 = \varepsilon. \tag{15}$$

The solution of (15) can be obtained by using eigendecomposition of $\boldsymbol{R}_{xx}$ similar to the approach in [22] and the diagonal loading term can be computed using a Newton-like algorithm. To prevent the negative, zero, or complex solution of (15), the following assumption is mandatory

$$\left\|\overline{\boldsymbol{a}}_0\right\|^2 > \varepsilon. \tag{16}$$

This technique undergoes the following limitations. First, eigendecomposition requires high computational burden of order $O(M^3)$. Additionally, the adaptive implementation updates both the covariance matrix and its inverse to compute the diagonal loading value and the robust detector, respectively. Second, this technique is based on batch algorithm and there is no clear vision for its recursive implementation even with

subspace tracking techniques. This is so because, the subspace tracking algorithms recursively update the eigenvectors and then at certain snapshot the current estimate is not the optimal eigenvectors and therefore the diagonal loading term will not be precisely computed which may lead to errors accumulation. Furthermore, the rank of signal and noise may be uncertain or not exactly known and need to be estimated prior to eigendecomposition. As a consequence, this technique is expected to fail in a dynamic interference scenario. Third, the technique reduces the inequality in (9) to equality which is not always accepted. More specifically, the diagonal of covariance matrix is *continuously* loaded even without mismatch.

B. Robust Capon Beamforming With Optimum VL

The first essence behind this paper is to develop an optimum VL approach to manage the uncertainty ellipsoidal constraint on the steering vector and hence to obtain the *genuine* steering vector from the *presumed* steering vector. The optimal diagonal loading term λ is precisely computed with low computational complexity using a VL approach instead of eigendecomposition or SOCP batch approaches. The method of steepest descent (SD) [9], [23] and the conjugate gradient (CG) method [24], [25] are invoked to recursively update the *genuine* steering vector that minimizes the Lagrangian functional (11) of robust Capon beamforming. This yields, respectively

$$\hat{\boldsymbol{a}}_{\mathbf{O}}(k) = \hat{\boldsymbol{a}}_{\mathbf{O}}(k-1) - \mu_{SD}(k)\boldsymbol{g}(k) \tag{17}$$

$$\hat{\boldsymbol{a}}_{\mathbf{O}}(k) = \hat{\boldsymbol{a}}_{\mathbf{O}}(k-1) - \mu_{CG}(k)\boldsymbol{p}(k) \tag{18}$$

where $\mu_{SD}(n)$ and $\mu_{CG}(n)$ are the step-sizes of the SD and CG algorithms respectively and $\boldsymbol{g}(k)$ is the conjugate derivative of $\Psi_{\hat{\boldsymbol{a}}_0}(k)$ with respect to $\hat{\boldsymbol{a}}_0^H(n)$ and can be computed as

$$\boldsymbol{g}(k) = \boldsymbol{R}_{xx}^{-1}(k)\hat{\boldsymbol{a}}_{\mathbf{O}}(k-1) + \lambda\left(\hat{\boldsymbol{a}}_{\mathbf{O}}(k-1) - \overline{\boldsymbol{a}}_0\right). \tag{19}$$

The direction vector $\boldsymbol{p}(n)$ can be computed as in [25]

$$\boldsymbol{p}(k+1) = \boldsymbol{g}(k) + \omega(k)\boldsymbol{p}(k) \tag{20}$$

where

$$\omega(k) = \frac{\left(\boldsymbol{g}(k) - \boldsymbol{g}(k-1)\right)^H \boldsymbol{g}(k)}{\boldsymbol{g}(k-1)^H \boldsymbol{g}(k-1)}. \tag{21}$$

The optimal step-sizes of the SD and CG algorithms can be obtained, respectively, by substituting (17) and (18) into (11) which engenders quadratic functions in the step-sizes with global minima [9], [25], [26]. As a consequence, the optimal step-sizes can be estimated, respectively, as

$$\mu_{SD}(k) = \frac{\alpha \boldsymbol{g}^H(k)\boldsymbol{g}(k)}{\boldsymbol{g}^H(k)\boldsymbol{R}_{xx}^{-1}(k)\boldsymbol{g}(k) + \sigma} \tag{22}$$

$$\mu_{CG}(k) = \frac{\alpha \boldsymbol{p}^H(k)\boldsymbol{g}(k-1)}{\boldsymbol{p}^H(k)\boldsymbol{R}_{xx}^{-1}(k)\boldsymbol{p}(k) + \sigma} \tag{23}$$

where α, σ are two positive constants added to improve the numerical stability of the algorithm. The constant α acts as dominant controller to the step-size range and should be set to suitable value while the constant σ can be set to a very small value (i.e., 10^{-6}).

The SD adaptive implementation of $\hat{\boldsymbol{a}}_{\mathbf{O}}(k)$ can be obtained by substituting (19) into (17)

$$\hat{\boldsymbol{a}}_{\mathbf{O}}(k) = \hat{\boldsymbol{a}}_{\mathbf{O}}(k-1) - \mu_{SD}(k)\left(\boldsymbol{R}_{xx}^{-1}(k)\hat{\boldsymbol{a}}_{\mathbf{O}}(k-1) + \lambda(k)\left(\hat{\boldsymbol{a}}_{\mathbf{O}}(k-1) - \overline{\boldsymbol{a}}_0\right)\right). \tag{24}$$

Correspondingly, the adaptive implementation of $\hat{\boldsymbol{a}}_{\mathbf{O}}(k)$ using the CG method is obtained by updating $\boldsymbol{p}(n+1)$ using (20) and then updating $\hat{\boldsymbol{a}}_{\mathbf{O}}(k+1)$ in the forthcoming iteration.

The spherical constraint in (10) should be satisfied at each iteration step, i.e., $\left\|\hat{\boldsymbol{a}}_{\mathbf{O}}(k) - \overline{\boldsymbol{a}}_0\right\|^2 \le \varepsilon$. Assuming the constraint was satisfied in the previous iteration and using (24), the following inequality is obtained:

$$\begin{aligned}&\left(\left(\tilde{\boldsymbol{a}}_0(k) - \mu_{SD}(k)\lambda(k)\left(\hat{\boldsymbol{a}}_0(k-1) - \overline{\boldsymbol{a}}_0\right)\right) - \overline{\boldsymbol{a}}_0\right)^H \\ &\quad\cdot\left(\left(\tilde{\boldsymbol{a}}_0(k) - \mu_{SD}(k)\lambda(k)\left(\hat{\boldsymbol{a}}_0(k-1) - \overline{\boldsymbol{a}}_0\right)\right) - \overline{\boldsymbol{a}}_0\right) \le \varepsilon\end{aligned} \tag{25}$$

where

$$\tilde{\boldsymbol{a}}_0(k) = \hat{\boldsymbol{a}}_0(k-1) - \mu_{SD}(k)\boldsymbol{R}_{xx}^{-1}(k)\hat{\boldsymbol{a}}_0(k-1). \tag{26}$$

From (25), we get

$$\begin{aligned}&\left\|\tilde{\boldsymbol{a}}_0(k) - \overline{\boldsymbol{a}}_0\right\|^2 - 2\mu_{SD}(k)\lambda(k)\left(\hat{\boldsymbol{a}}_0(k-1) - \overline{\boldsymbol{a}}_0\right)^H \\ &\cdot\left(\tilde{\boldsymbol{a}}_0(k) - \overline{\boldsymbol{a}}_0\right) + \mu_{SD}^2(k)\lambda(k)^2\left\|\hat{\boldsymbol{a}}_0(k-1) - \overline{\boldsymbol{a}}_0\right\|^2 \le \varepsilon.\end{aligned} \tag{27}$$

Therefore, if the spherical constraint is not achieved, i.e., $\left\|\hat{\boldsymbol{a}}_{\mathbf{O}}(k) - \overline{\boldsymbol{a}}_0\right\|^2 > \varepsilon$, we solve for equality in (27). Specifically, the steering vector $\tilde{\boldsymbol{a}}_0(k)$ is dragged to be on the boundary of the constraint. Otherwise, the updated steering vector is accepted and the algorithm resumes to the forthcoming step. Subsequently, the value for $\lambda(k)$ satisfying the spherical constraint is

$$\lambda(k) = \frac{b_1 \pm \sqrt{b_1^2 - a_1 c_1}}{a_1} \tag{28}$$

where

$$\begin{aligned}a_1 &= \mu_{SD}^2(k)\left\|\hat{\boldsymbol{a}}_0(k-1) - \overline{\boldsymbol{a}}_0\right\|^2 > 0 \\ b_1 &= \mu_{SD}(k)\mathrm{Re}\left\{\left(\tilde{\boldsymbol{a}}_0(k) - \overline{\boldsymbol{a}}_0\right)^H\left(\hat{\boldsymbol{a}}_0(k-1) - \overline{\boldsymbol{a}}_0\right)\right\} \\ c_1 &= \left\|\tilde{\boldsymbol{a}}_0(k) - \overline{\boldsymbol{a}}_0\right\|^2 - \varepsilon > 0.\end{aligned} \tag{29}$$

To prevent complex roots solution of (27), we plug (26) and (29) into $b_1^2 - a_1 c_1 \ge 0$, and hence the following inequality is obtained

$$\begin{aligned}&\left[\mathrm{Re}\left\{\left(\boldsymbol{d}_0(k-1) - \mu_{SD}\overline{\boldsymbol{g}}(k)\right)\left(\boldsymbol{d}_0(k-1)\right)\right\}\right]^2 \\ &\quad\ge \left\|\boldsymbol{d}_0(k-1)\right\|^2\left[\left(\boldsymbol{d}_0(k-1) - \mu_{SD}\overline{\boldsymbol{g}}(k)\right)^H\right. \\ &\quad\quad\left.\cdot\left(\boldsymbol{d}_0(k-1) - \mu_{SD}\overline{\boldsymbol{g}}(k)\right) - \varepsilon\right]\end{aligned} \tag{30}$$

where

$$\overline{\boldsymbol{g}}(k) = \boldsymbol{R}_{xx}^{-1}(k)\hat{\boldsymbol{a}}_0(k-1) \tag{31}$$

$$\boldsymbol{g}(k) = \overline{\boldsymbol{g}}(k) + \lambda(k)\left(\hat{\boldsymbol{a}}_0(k-1) - \overline{\boldsymbol{a}}_0\right) \tag{32}$$

$$\boldsymbol{d}_0(k-1) = \hat{\boldsymbol{a}}_0(k-1) - \overline{\boldsymbol{a}}_0. \tag{33}$$

In order to simplify (30) which contains complex vectors, it should be converted to real-valued inequality as in [11]. By defining the following real vectors:

$$\breve{\boldsymbol{d}}_0(k-1) = \left[\mathrm{Re}\left\{\boldsymbol{d}_0(k-1)\right\}^T, \mathrm{Im}\left\{\boldsymbol{d}_0(k-1)\right\}^T\right] \quad (34)$$

$$\breve{\boldsymbol{g}}(k) = \left[\mathrm{Re}\left\{\overline{\boldsymbol{g}}(k)\right\}^T, \mathrm{Im}\left\{\overline{\boldsymbol{g}}(k)\right\}^T\right]. \quad (35)$$

Then by injecting (34) and (35) into (30) and converting it to real-valued inequality, we get

$$\left[\left(\breve{\boldsymbol{d}}_0(k-1) - \mu_{SD}\breve{\boldsymbol{g}}(k)\right)^T\left(\breve{\boldsymbol{d}}_0(k-1)\right)\right]^2 \geq \left\|\breve{\boldsymbol{d}}_0(k-1)\right\|^2 \cdot \left[(\breve{\boldsymbol{d}}_0(k-1) - \mu_{SD}\breve{\boldsymbol{g}}(k))^T(\breve{\boldsymbol{d}}_0(k-1) - \mu_{SD}\breve{\boldsymbol{g}}(k)) - \varepsilon\right]. \quad (36)$$

After some manipulations to (36), the following step-size upper bound is obtained, shown in (37) at the bottom of the page. Analogous steps can be acquired for the CG algorithm. More interestingly, the proposed implementation using VL technique can be extended to include the flat ellipsoidal constraint proposed in [13] and even the optimization problem in [12] can be solved using the Lagrange method and, hence, it can be on-line implemented using the proposed methodology.

C. Cooperative Joint Constraint Approach

The robust Capon beamformer in (8) exhibits some performance degradation at low SNR. This can be further clarified from (8) "the maximization of the power after the interference has been declined"

$$\max_{\hat{\boldsymbol{a}}_0} \hat{\boldsymbol{w}}_0^H \boldsymbol{R}_{xx}\hat{\boldsymbol{w}}_0\Big|_{\boldsymbol{R}_{xx}=\sum_{i=1}^{L}\boldsymbol{\rho}_i\boldsymbol{s}_i\boldsymbol{s}_i^H+\boldsymbol{R}_v} \Rightarrow \max_{\hat{\boldsymbol{a}}_0}\left(\hat{\boldsymbol{w}}_0^H\sum_{i=1}^{L}\boldsymbol{\rho}_i\boldsymbol{s}_i\boldsymbol{s}_i^H\hat{\boldsymbol{w}}_0 + \sigma_v^2\hat{\boldsymbol{w}}_0^H\hat{\boldsymbol{w}}_0\right) \quad (38)$$

where $\hat{\boldsymbol{w}}_0$ is the optimal robust Capon beamformer with ellipsoidal/spherical constraint on the steering vector, $\boldsymbol{s}_i$ and $\boldsymbol{\rho}_i$ signify, respectively, the effective steering vector and the power of source i, and $\boldsymbol{R}_v = \sigma_v^2\boldsymbol{I}_M$ denotes the component of the data covariance matrix due to random noise.

Therefore, the above optimization problem includes spontaneous maximization of the noise constituent $\sigma^2\hat{\boldsymbol{w}}_0^H\hat{\boldsymbol{w}}_0$. In order to mitigate the effect of noise enhancement, we can impose a quadratic constraint on the weight vector norm. In addition to this, the proposed beamformer may attain other merits of the quadratic constraint such as robustness to pointing errors and random perturbation in detector parameters and small training sample size [8], [9], [17], [27]. To start the formulation of this constraint, we directly impose the quadratic constraint on the robust Capon beamformer obtained under ellipsoidal uncertainty set, i.e.

$$\min_{\hat{\boldsymbol{w}}_0}\hat{\boldsymbol{w}}_0^H\boldsymbol{R}_{xx}\hat{\boldsymbol{w}}_0 \text{ subject to } \hat{\boldsymbol{w}}_0^H\hat{\boldsymbol{a}}_0(\theta_0) = 1;\ \hat{\boldsymbol{w}}_0^H\hat{\boldsymbol{w}}_0 \leq \tau \quad (39)$$

where $\hat{\boldsymbol{a}}_0(\theta_0)$ is the *genuine* steering vector and can be updated using (17) or (18). The solution to this optimization problem can be obtained using the method of Lagrange multiplier as [8], [9], [22]

$$\tilde{\boldsymbol{w}}_0 = \frac{\left(\boldsymbol{R}_{xx} + \upsilon\boldsymbol{I}_M\right)^{-1}\hat{\boldsymbol{a}}_0(k)}{\hat{\boldsymbol{a}}_0^H(k)\left(\boldsymbol{R}_{xx} + \upsilon\boldsymbol{I}_M\right)^{-1}\hat{\boldsymbol{a}}_0(k)}. \quad (40)$$

Two variable loading techniques are proposed in [8] and [9] to get the optimum diagonal loading term. Regrettably, these approaches are basically developed using the generalized sidelobe canceller (GSC) structure which would not be appropriated here due to the first optimization problem (8). More specifically, the optimization problem in (8) includes *genuine* steering vector optimization, that is, the upper quiescent vector of GSC structure should be optimized concurrently with the lower portion. This dual optimization problem seems to be problematical with GSC structure. Therefore, we have to adopt a direct form realization. Unfortunately, direct solution of (39) seems to be complicated as well due to the existence of the diagonal loading term in both numerator and denominator of (40). To overcome this difficulty, we can take the diagonal loading term out from the denominator of (40). This key assumption can be recognized thanks to the denominator of (40) has been already optimized in (8). As a result, the optimum solution can be computed as

$$\breve{\boldsymbol{w}}_0 = \frac{\left(\boldsymbol{R}_{xx} + \upsilon\boldsymbol{I}_M\right)^{-1}\hat{\boldsymbol{a}}_0(k)}{\hat{\boldsymbol{a}}_0^H(k)\boldsymbol{R}_{xx}^{-1}\hat{\boldsymbol{a}}_0(k)}. \quad (41)$$

By substituting (12) into (41), a closed-form solution for the joint-constraint beamformer can be obtained

$$\breve{\boldsymbol{w}}_0 = \frac{\left(\boldsymbol{R}_{xx} + \upsilon\boldsymbol{I}_M\right)^{-1}\boldsymbol{R}_{xx}\left(\boldsymbol{R}_{xx} + \frac{\boldsymbol{I}_M}{\lambda}\right)^{-1}\overline{\boldsymbol{a}}_0}{\overline{\boldsymbol{a}}_0^H\left(\boldsymbol{R}_{xx} + \frac{\boldsymbol{I}_M}{\lambda}\right)^{-1}\boldsymbol{R}_{xx}\left(\boldsymbol{R}_{xx} + \frac{\boldsymbol{I}_M}{\lambda}\right)^{-1}\overline{\boldsymbol{a}}_0}. \quad (42)$$

The above closed-form solution contains two positive diagonal loading terms. The first diagonal loading term λ can be obtained using the proposed VL technique in Section III.B. The

$$\mu_{SD} \leq \sqrt{\frac{\varepsilon\left\|\breve{\boldsymbol{d}}_0(k-1)\right\|^2}{\left[\left\|\breve{\boldsymbol{d}}_0(k-1)\right\|^2\|\breve{\boldsymbol{g}}(k)\|^2 - \breve{\boldsymbol{g}}^H(k)\breve{\boldsymbol{d}}_0(k-1)\breve{\boldsymbol{d}}_0(k-1)^H\breve{\boldsymbol{g}}(k)\right]}}. \quad (37)$$

Taylor series approximation originally proposed in [5] and further adopted in [8] can be invoked to obtain the second diagonal loading term υ as follows:

$$\breve{\boldsymbol{w}}_0 = \frac{\left(\boldsymbol{I}_M + \upsilon \boldsymbol{R}_{xx}^{-1}\right)^{-1} \boldsymbol{R}_{xx}^{-1}\hat{\boldsymbol{a}}_0(k)}{\hat{\boldsymbol{a}}_0^H(k)\boldsymbol{R}_{xx}^{-1}\hat{\boldsymbol{a}}_0(k)} \approx \frac{\left(\boldsymbol{I}_M - \upsilon \boldsymbol{R}_{xx}^{-1}\right)\boldsymbol{R}_{xx}^{-1}\hat{\boldsymbol{a}}_0(k)}{\hat{\boldsymbol{a}}_0^H(k)\boldsymbol{R}_{xx}^{-1}\hat{\boldsymbol{a}}_0(k)} \Rightarrow \breve{\boldsymbol{w}}_0 \approx \hat{\boldsymbol{w}}_0 - \upsilon \boldsymbol{w}_0 \quad (43)$$

where

$$\boldsymbol{w}_0 = \boldsymbol{R}_{xx}^{-1}\hat{\boldsymbol{w}}_0. \quad (44)$$

Therefore, utilizing the quadratic constraint in (39) with the last update equation in (43), the diagonal loading term υ can be obtained using a simple quadratic equation [8]. It is really interesting to highlight the drawback of the Taylor series approximation in (43), that is, the diagonal loading term υ can not be precisely computed due to this approximation and even real diagonal loading can not be guaranteed [8], [9]. Nevertheless, consolidating the two approaches generate extremely robust beamformer especially at low SNR which will be demonstrated in Section IV.

D. On-Line Adaptive Implementation

As an outline for the adaptive algorithm; the matrix $\boldsymbol{R}_{xx}^{-1}(k)$ is updated using the well-known RLS algorithm as shown in Fig. 1. The unconstrained steering vector $\tilde{\boldsymbol{a}}_0(k)$ is updated using (17) or (18). If $\tilde{\boldsymbol{a}}_0(k)$ does not fulfill the ellipsoidal constraint, then the optimal loading is calculated using (28) and the genuine steering vector $\hat{\boldsymbol{a}}_0(k)$ is obtained as

$$\hat{\boldsymbol{a}}_0(k) = \tilde{\boldsymbol{a}}_0(k) - \mu_{SD|CG}(k)\lambda(k)\left(\hat{\boldsymbol{a}}_0(k-1) - \overline{\boldsymbol{a}}\right). \quad (45)$$

This VL technique depends only on the difference between $\hat{\boldsymbol{a}}_0(k-1)$ and the *presumed* steering vector. Consequently, the optimal diagonal loading term in (45) requires $O(M)$ complexity. Compared with previously published robust techniques, the new robust technique has a considerable lower complexity whereas; the SOCP [12] and eigendecomposition [13] approaches require at least $O(M^3)$ flops. Substituting (45) into (13), the robust beamformer $\hat{\boldsymbol{w}}_0$ with single ellipsoidal constraint is obtained.

The joint constraint beamformer and the single constraint beamformer are outlined in Fig. 1. The joint constraint beamformer $\breve{\boldsymbol{w}}_0$ can be obtained by solving a simple quadratic equation as depicted in Fig. 1. The total amount of the required multiplications at each snapshot for the single and joint constraint beamformers is $O(3M^2+10M)$ and $O(4M^2+13M)$, respectively, as shown in Fig. 1.

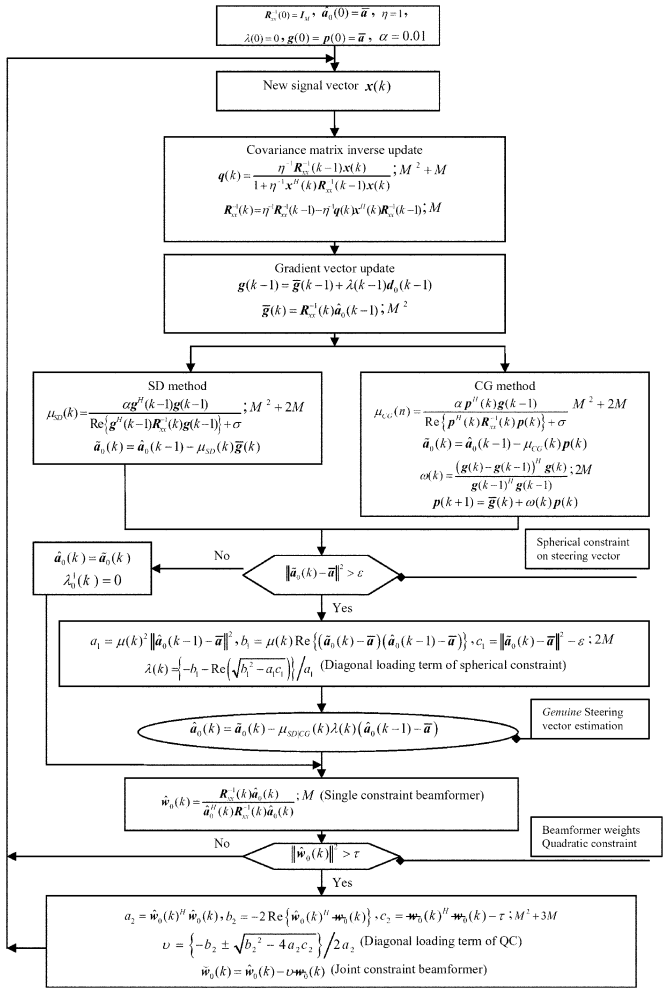

Fig. 1. Flowchart of the proposed robust Capon beamformers with the required amount of multiplications at each step.

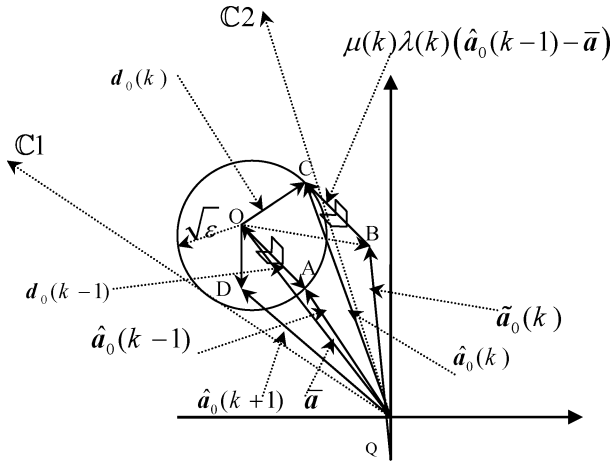

Fig. 2. Geometric representation of robust Capon beamforming with ellipsoidal constraint.

E. Geometric Explanation

To elucidate the proposed robust adaptive Capon beamformer algorithm with spherical constraint, a simple 2-D case is adopted as portrayed in Fig. 2. The center point Q is the array reference point. The steering vector $\overline{\boldsymbol{a}}$ $(\overrightarrow{QO})$ represents the *presumed* steering vector. The circle centered at O embodies the spherical constraint $\left\|\hat{\boldsymbol{a}}_0(k) - \overline{\boldsymbol{a}}\right\|^2 \le \varepsilon$. The bounded area by the circle and the two lines $\mathbb{C}1$, $\mathbb{C}2$ exemplify the constrained vicinity within the constrained value ε. In a 3-D case, this area is bounded by a sphere centered at origin O and a cone with nape at Q.

Assuming the preceding *genuine* steering vector $\hat{\boldsymbol{a}}_0(k-1)$ $(\overrightarrow{QA})$ located inside the constrained vicinity. After next iteration, the steering vector $\tilde{\boldsymbol{a}}_0(k)$ $(\overrightarrow{QB})$ is updated using (26) which may be located outside the constrained region i.e., $\|\tilde{\boldsymbol{a}}_0(k)-\overline{\boldsymbol{a}}\|^2 > \varepsilon$. Then, the variable loading technique is invoked and the diagonal loading term is computed using (28) and the term $\mu(k)\lambda(k)(\hat{\boldsymbol{a}}_0(k-1)-\overline{\boldsymbol{a}})$ $(\overrightarrow{BC})$ is appended to the steering vector to obtain the new constrained steering vector $\hat{\boldsymbol{a}}_0(k)$ $(\overrightarrow{QC})$ which fulfills the spherical constraint ($\|\hat{\boldsymbol{a}}_0(k)-\overline{\boldsymbol{a}}\|^2 = \varepsilon$). If the recent steering vector $\hat{\boldsymbol{a}}_0(k+1)$ $(\overrightarrow{QD})$ is located inside the constrained area the algorithm resumes without carrying out the VL subroutine. Therefore, this technique is fully achieving the inequality constraint $\|\hat{\boldsymbol{a}}_0(k)-\overline{\boldsymbol{a}}\|^2 \leq \varepsilon$ using loading-on-demand mechanism while the eigendecomposition approach proposed in [13] reduced it to equality and subsequently *continuously* loading the diagonal of the data covariance matrix. For example, the steering vector $\hat{\boldsymbol{a}}_0(k+1)$ will be dragged to be on the constrained boundary (i.e., the circle in the figure) although it is located inside the constrained area.

IV. Simulations Results

In this section, computer simulations are carried out to investigate the performance of the proposed beamformers. Consider 5-element uniform linear array with half wavelength element spacing. We consider the look direction of the desired source at broadside (i.e., $DOA = 0°$) with 0 dB power. Assuming isotropic element and ignoring mutual coupling effect between elements. There are two equipowered interferers are located at $\varphi_1 = \pi/6$ and $\varphi_2 = \pi/4$ with 10 dB power to simulate the near-far effect. The noise-power at each antenna element is -40 dB.

The performance of the proposed single constraint beamformer (referred to as Proposed 1) and the joint constraint beamformer (referred to as Proposed 2) along with the traditional Capon beamformer (referred to as; standard Capon) and the robust Capon beamformer proposed in [13] [referred to as robust Capon (batch)] are assessed in this experiment. The robust Capon (batch) beamformer is adapted using the batch algorithm proposed [13]. Moreover, a recursive implementation of robust Capon (batch) beamformer using subspace tracking algorithm [referred to as robust Capon (SS)] is also simulated. Two versions of the normalized orthogonal Oja (NOOja) algorithm proposed in [26] are used to track both signal (principal eigenvectors) and noise (minor eigenvectors) subspaces. The eigenvalues are calculated using batch mode (i.e., $\boldsymbol{\Gamma}(k) = \boldsymbol{U}^H(k)\boldsymbol{R}_{xx}(k)\boldsymbol{U}(k)$) to improve the performance of robust Capon (SS) beamformer. In addition to this, the robust beamformer proposed in [12] based on SOCP [referred to as robust Capon (SOCP)] is also incorporated in simulation. The performance of aforementioned beamformers is assessed in terms of output SINR, mean squared error (MSE) between the array output signal and the desired source signal, and SOIP, all versus snapshots and the steady state beampatterns of the antenna array against DOA. For the SOCP, the presumed steering vector is normalized as $\overline{\boldsymbol{a}}_0 = M(\overline{\boldsymbol{a}}_0/\|\overline{\boldsymbol{a}}_0\|)$ [12].

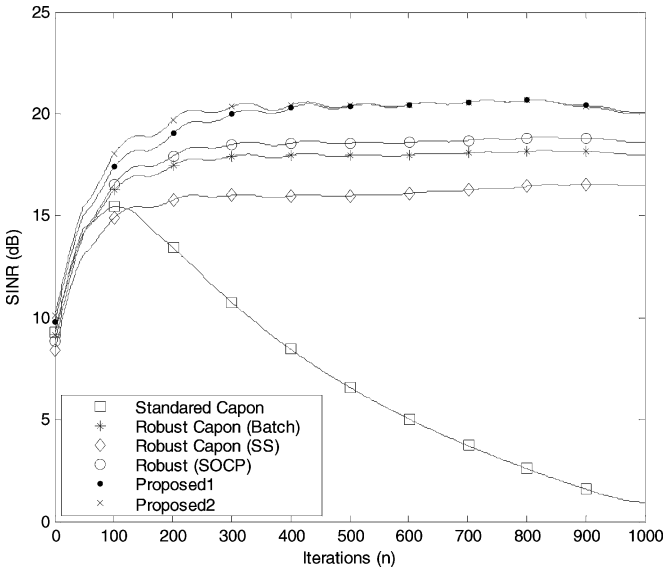

Fig. 3. Output SINR versus snapshot for first scenario.

In order to corroborate the robustness of the proposed algorithms, two simulation scenarios are conducted. In the first scenario, there is $0.03\pi = 5.4°$ DOA mismatch. The ellipsoidal constrained value (ε) is set to 0.5 for all beamformers except robust Capon (SOCP) beamformer is set to 1.5 due to the normalization step required by SOCP algorithm (see [12] for more information). The selection of these constrained values is the best for all beamformer with this scenario. These constrained values are relative to the DOA mismatch upper bound and obtained empirically using numerous simulations runs. In the second scenario, there is $0.06\pi = 10.8°$ DOA mismatch. The constrained values are set to one for all beamformers and 2 for SOCP. The quadratic inequality constraint value is set to $\tau = 0.2$ in the two scenarios. In the second scenario, the noise-power at each antenna element is increased to be -20 dB. The first scenario is adapted using the SD method while the CG method is exercised in the second scenario. All figures are obtained by averaging 50 autonomous runs.

Figs. 3–5 demonstrate the output SINR, SOIP, and MSE for the six competing beamformers with the first scenario. The steady state beampatterns are shown in Fig. 6. For clarity, the joint constraint beamformer is excluded from Fig. 6 as it is similar to the single constraint beamformer in steady state performance as manifest from Fig. 3. It is evident from Fig. 3 that the proposed algorithms offer about 2 dB improvement in output SINR over the robust Capon (SOCP) beamformer. Notwithstanding the deployment of fast subspace tracking algorithm, the robust Capon (SS) beamformer undergoes performance degradation with regard to robust Capon (batch) beamformer. The robust Capon (batch) and robust Capon (SS) beamformers offer the maximum SOIP as shown in Fig. 4. This is, not astonishingly, due to *continuous* loading of data covariance matrix. However, SOIP is not the precise performance indicator. Fig. 5 demonstrates that the proposed beamformers exhibit the minimum MSE performance and hence they offer best signal tracking capability. It is clear from Fig. 6 that the proposed beamformer offers the highest desired signal beam

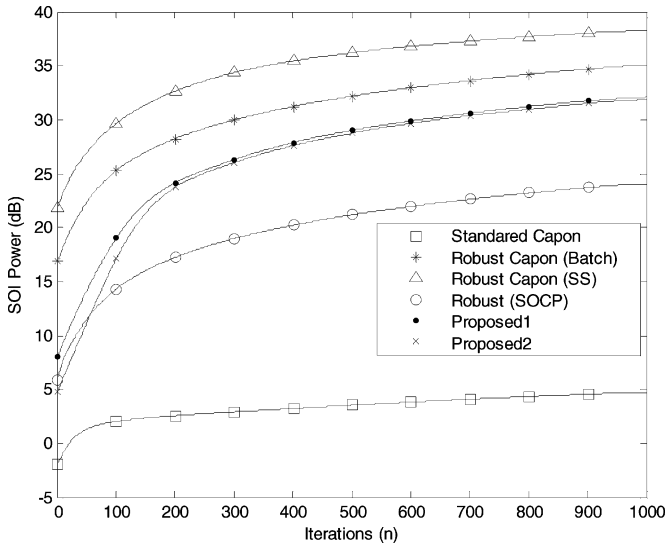

Fig. 4. SOI power versus snapshot for first scenario.

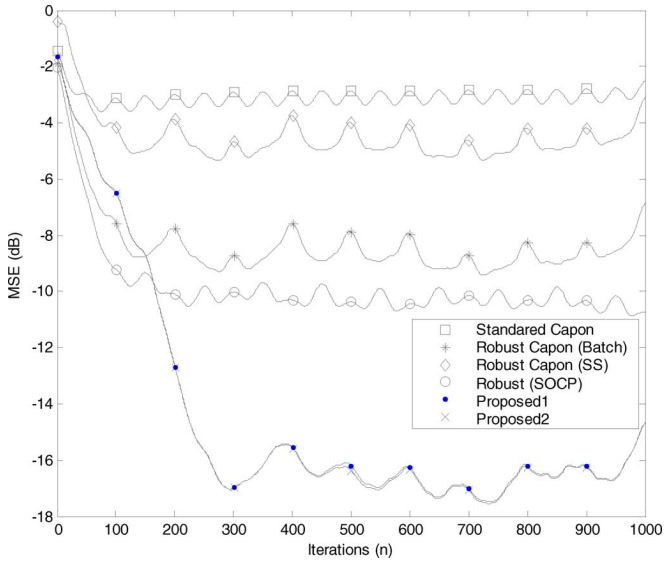

Fig. 5. Mean squared error versus snapshot for first scenario.

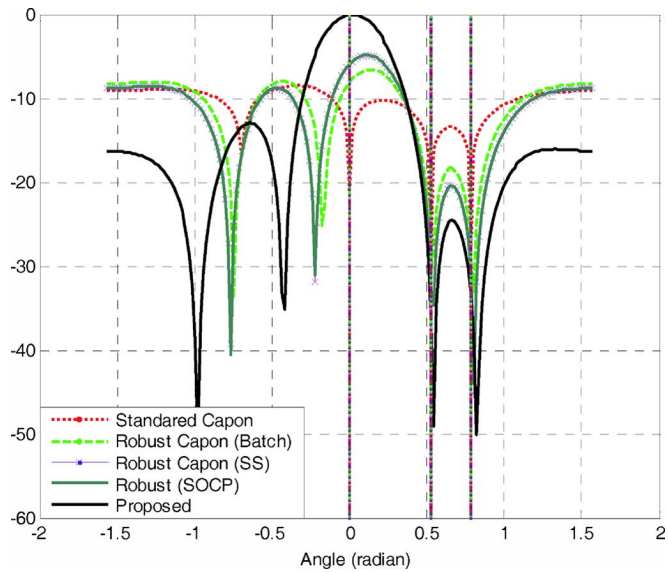

Fig. 6. Steady state beampatterns for the first scenario.

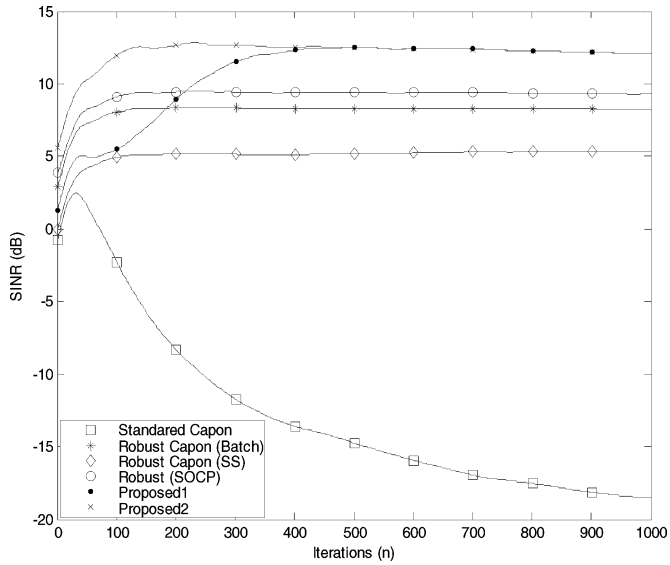

Fig. 7. Output SINR versus snapshot for the second scenario.

and has deep nulls at interferers DOA comparable to other robust approaches. Moreover, the proposed beamformer exhibits the best sidelobe suppression competence. The performance of the Standard Capon beamformer substantially degraded due to DOA mismatch. As a final point, the performance of single and joint constraints beamformers are almost similar with the first scenario due to high SNR as shown in Fig. 3.

Fig. 7 illustrates the output SINR with the second scenario while other figures are similar to first scenario. The general look of Fig. 7 is similar to Fig. 3 except the single constraint beamformer has initial performance degradation in terms of slow convergence rate.

It is appealing now to inspect the behaviors of the beamformers against noise power. Figs. 8 and 9 demonstrate the steady state of output SINR versus noise power for the six aforementioned beamformers with the two simulation scenarios, correspondingly. The figures illustrate that the proposed beamformers achieve the best SINR over wide range of noise power. The joint constraint beamformer offers little improvement over the single constraint beamformer particularly at low SNR.

A. *Mutual Coupling Effect*

In the above scenarios, the antenna array is assumed to be ideal, that is, the position and electrical characteristics of antenna elements are accurate. However, in real systems, these assumptions are not much satisfied due to the uncertainties of element position and violation of isotropic assumption (due to reradiating the incident signal, nonidentical elements, antenna aging, etc) and subsequently mutual coupling between array elements become significant. Therefore, it is worthwhile to study mutual coupling effect on the performance of the beamforming algorithms.

To examine the effect of mutual coupling, three experiments based on element spacing and noise power are simulated. The

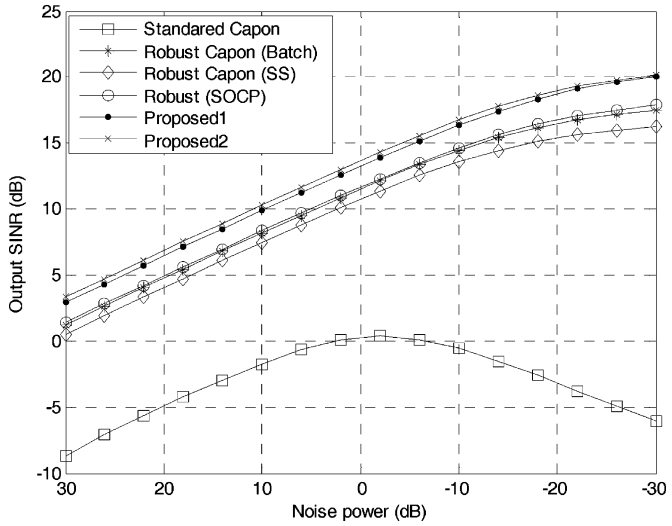

Fig. 8. Output SINR versus noise power with 0.03π mismatch.

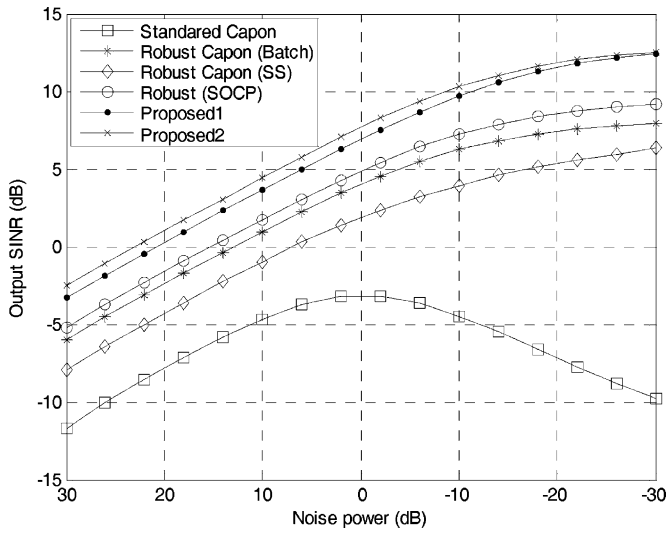

Fig. 9. Output SINR versus noise power with 0.06π mismatch.

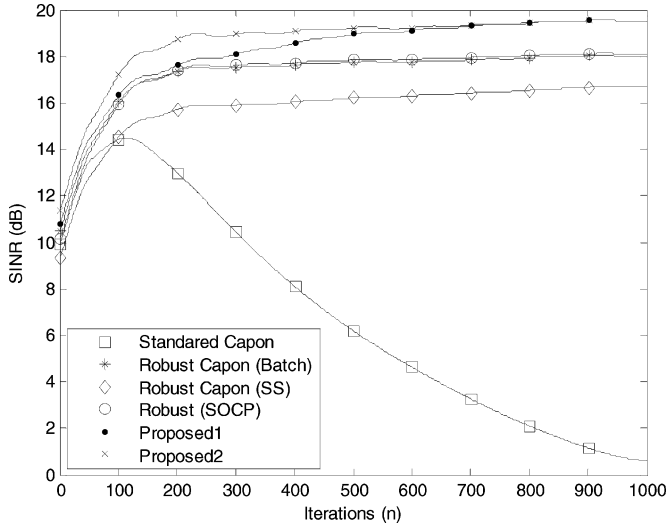

(a)

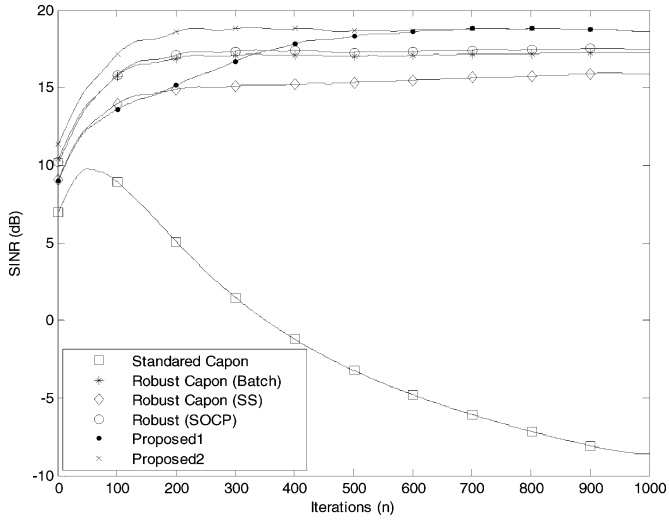

(b)

Fig. 10. (a) Output SINR with 0.5λ element spacing and $\mathrm{SNR} = 40$. (b) Output SINR with 0.5λ element spacing and $\mathrm{SNR} = 30$.

first simulation scenario is tested with three element spacing (0.5λ, 0.4λ and 0.3λ) in presence of mutual coupling with both 40 dB and 30 dB noise powers. The mutual impedance matrix $\boldsymbol{Z}$ is computed using the Matlab script provided in [20] and the mutual coupling matrix is calculated using (3). Figs. 10–12 illustrate the performance of the competing beamformers with 0.5λ, 0.4λ, and 0.3λ element spacing respectively.

The following remarks are observed from the figures:

1) The performance of all beamformers except the proposed beamformers is degraded when element spacing decreases (i.e., mutual coupling increasing).
2) A performance degradation of robust Capon (SOCP) beamformer at low SNR is noticeable at significant mutual coupling.
3) At significant mutual coupling, the performance of the single constraint beamformer converges to the joint constraint beamformer, and the initial degradation of the single constraint beamformer is shrunk.
4) Among the simulated robust beamformers, the robust Capon (SS) beamformer is the seriously degraded beamformer with mutual coupling increasing.

B. Moving Jamming Effect

Finally, the effect of moving interferers on the performance of the beamformers is examined. Two moving interferers' scenarios are considered. The first scenario is referred to as the stationary scenario and divided into two sub-scenarios. The trajectories of the interferers' motion versus snapshoot index $\boldsymbol{k}$ for the first scenario are as follows [28]–[30]:

$$\varphi_1 = \frac{\pi}{6} \pm 0.01\frac{\pi}{180}k, \quad \varphi_2 = \frac{\pi}{4} + 0.1\frac{\pi}{180}k. \tag{46}$$

The plus sign in the first interferer trajectory models a non-coherent jamming sub-scenario while the minus sign simulates a coherent jamming sub-scenario. The second scenario is referred

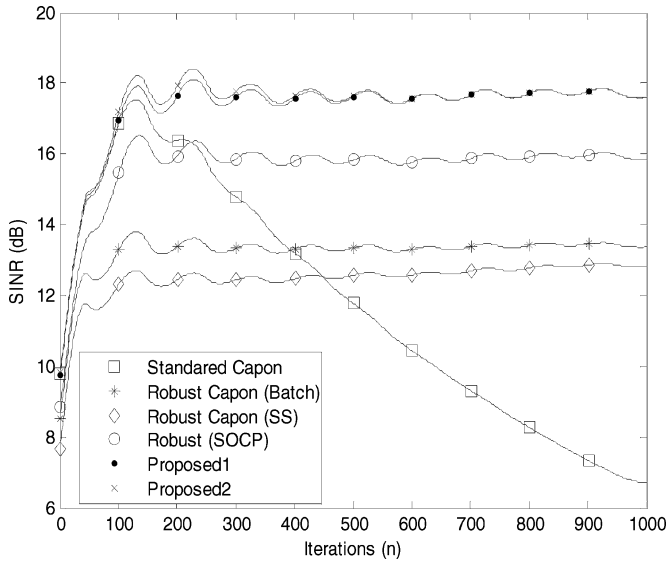

(a)

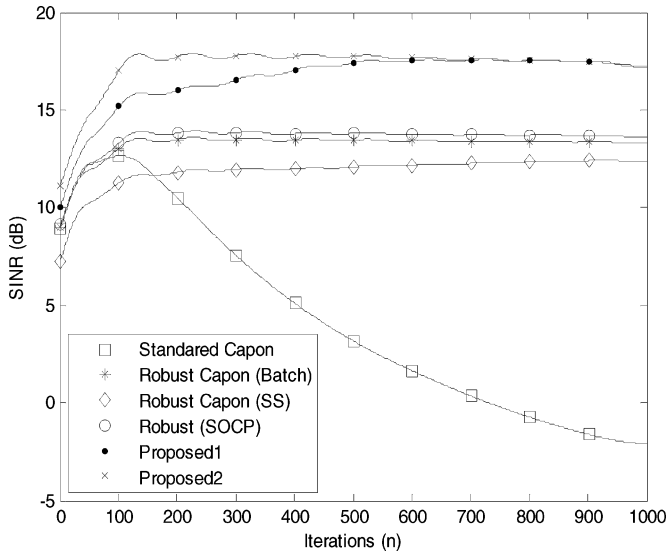

(b)

Fig. 11. (a) Output SINR with element spacing and $\mathrm{SNR} = 40$. (b) Output SINR with 0.4λ element spacing and $\mathrm{SNR} = 30$.

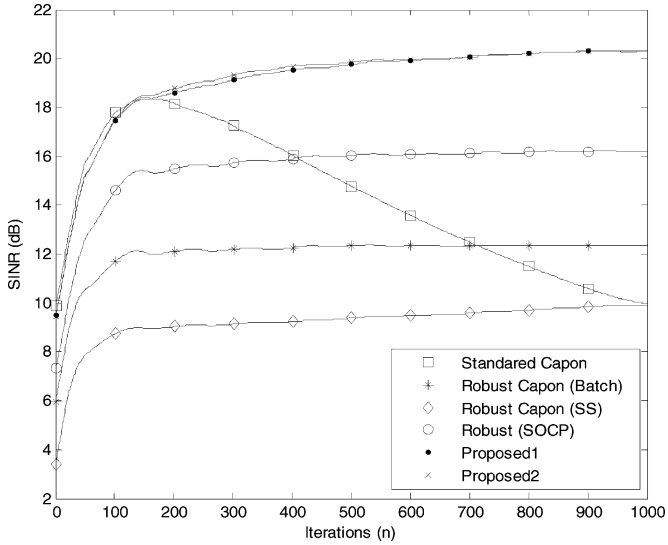

(a)

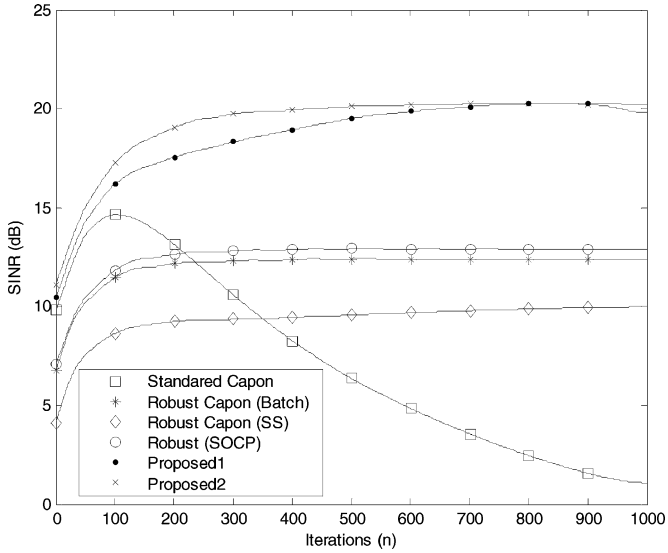

(b)

Fig. 12. (a) Output SINR with 0.3λ element spacing and $\mathrm{SNR} = 40$.(b) Output SINR with 0.3λ element spacing and $\mathrm{SNR} = 30$.

to as the non-stationary scenario and its jammers trajectories are as follows [16]:

$$\varphi_1 = \frac{\pi}{6} + 10 \times \frac{\pi}{180} \sin\left(\frac{k}{15}\right),\ \varphi_2 = \frac{\pi}{4} + 10 \times \frac{\pi}{180} \sin\left(\frac{k}{15}\right). \tag{47}$$

In addition, a 0.01π DOA mismatch is added in order to model a full dynamic scenario. The steering vectors of the interferers and hence the system matrix are time varying. The joint constraint approach is excluded from this simulation as it does not appear to offer any additional performance improvement over the single constraint approach. To confirm the previous hypothesis the noise-power is set to -20 dB at each antenna element. Figs. 13 and 14 demonstrate, respectively, the non-coherent and coherent sub-scenarios while Fig. 15 illustrates the non-stationary scenario.

It is apparent from Fig. 13 that the non-coherent jamming sub-scenario has minor impact on the anticipated algorithm. In addition, an incredible improvement is achieved by the proposed algorithm especially at high snapshoot index values. This is because the proposed algorithm possesses the best sidelobe suppression capability over wide range from possible interferers DOA as evident from Fig. 6. Degradation in performance for all beamformers is evident with coherent moving sub-scenario as shown in Fig. 14. However, the proposed algorithm has a graceful degradation in performance in the presence of coherent jamming. The nonstationary scenario introduces a little weaving in the steady state performance. However, it is evident from Fig. 15 that the proposed approach offers about 2 dB improvement over robust Capon (SOCP) beamformer. It is noteworthy that the robust Capon (SOCP) beamformer experiences considerable degradation with stationary scenario compared with other

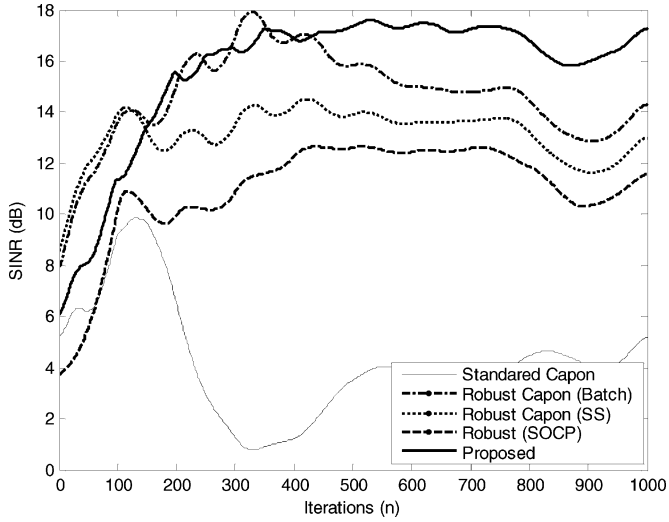

Fig. 13. Output SINR for non-coherent stationary moving sub-scenario.

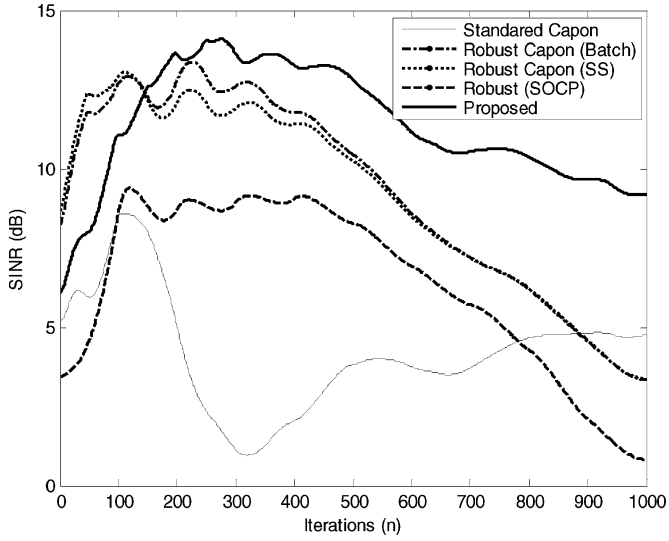

Fig. 14. Output SINR for coherent stationary moving sub-scenario.

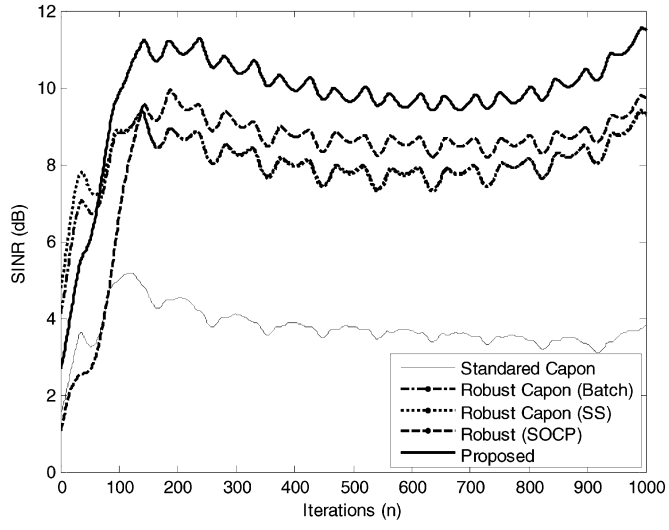

Fig. 15. Output SINR versus snapshot for non-stationary moving scenario.

robust approaches. This is because, the robust Capon (SOCP) beamformer is not robust against low SNR as demonstrated in mutual coupling simulation. However, it comes back on track next to the proposed approach with the nonstationary scenario.

V. Conclusion

In this paper we have proposed a new low-computational complexity recursive implementation for the robust Capon beamformer with uncertainty ellipsoidal constraint. Additionally, we proposed a joint constraint approach to improve the performance of the single constraint beamformer at low SNR. We verified from computer simulations that the overall performance of the proposed adaptive algorithms outperform other robust beamformers. Moreover, the proposed algorithms demonstrate superior attitude against mutual coupling and moving jamming while the performance of other robust approaches are unstable and unpredictable. In addition to the offered improvements relative to other robust approaches, the proposed algorithms exhibit also the following merits. The diagonal loading terms are precisely computed using VL technique. The inverse covariance matrix is merely updated and hence, the order of computational complexity of these robust approaches is comparable to the conventional beamformer. Future work may analyze other scenarios such as near field effect, local scattering, and wave front distortion.

References

[1] L. J. Griffiths and C. W. Jim, "An alternative approach to linearly constrained adaptive beamforming," *IEEE Trans. Antennas Propag.*, vol. AP–30, pp. 27–34, Jan. 1982.

[2] N. K. Jablon, "Adaptive beamforming with generalized sidelobe canceller in the presence of array imperfections," *IEEE Trans. Antennas Propag.*, vol. AP-34, pp. 996–1201, Aug. 1986.

[3] C. Y. Tseng and L. J. Griffiths, "A unified approach to the design of linear constraints in minimum variance adaptive beamformers," *IEEE Trans. Antennas Propag.*, vol. 40, pp. 1533–1542, Dec. 1992.

[4] Y. Lee and W.-R. Wu, "A robust adaptive generalized sidelobe canceller with decision feedback," *IEEE Trans. Antennas Propag.*, vol. 53, no. 11, pp. 3822–3832, Nov. 2005.

[5] M. W. Ganz, R. L. Moses, and S. L. Wilson, "Convergence of the SMI and diagonally loaded SMI algorithm with weak interference," *IEEE Trans. Antennas Propag.*, vol. 38, no. 3, Mar. 1990.

[6] B. Carlson, "Equivalence of adaptive array diagonal loading and omnidirectional jamming," *IEEE Trans. Antennas Propag.*, vol. 43, no. 5, pp. 540–541, May 1995.

[7] X. Mestre and M. A. Lagunas, "Diagonal loading for finite sample size beamforming: An asymptotic approach," in *Robust Adaptive Beamforming*. Hoboken, NJ: Wiley, 2006.

[8] Z. Tian, K. L. Bell, and H. L. Van Trees, "A recursive least squares implementation for LCMP beamforming under quadratic constraint," *IEEE Trans. Signal Processing.*, vol. 49, pp. 1138–1145, Jun. 2001.

[9] A. Elnashar, S. Elnoubi, and H. Elmikati, "A robust quadratically constrained adaptive blind multiuser receiver for DS/CDMA systems," in *Proc. 8th ISSSTA*, Sydney, Australia, 2004, pp. 164–168.

[10] A. Elnashar, "Robust adaptive beamforming," presented at the ACE2 Network of Excellence Workshop on Smart Antennas, MIMO Systems and Related Technologies, Mykonos, Greece, Jun. 8, 2006.

[11] A. Elnashar, S. Elnoubi, and H. Elmikati, "Robust adaptive beamforming with variable diagonal loading," in *Proc. 6th IEE Int. Conf. 3G & Beyond*, Nov. 2005, pp. 489–493.

[12] S. A. Vorobyov, A. B. Gershman, and Z.-Q. Luo, "Robust adaptive beamforming using worst-case performance optimization," *IEEE Trans. Signal Processing*, vol. 51, pp. 313–324, Feb. 2003.

[13] J. Li, P. Stoica, and Z. Wang, "On robust Capon beamforming and diagonal loading," *IEEE Trans. Signal Processing*, vol. 51, no. 7, pp. 1702–1715, Jul. 2003.

[14] J. F. Sturm, "Using SeDuMi 1.02, a MATLAB toolbox for optimization over symmetric cones," *Optim. Meth. Software*, vol. 11–12, pp. 625–653, Aug. 1999.

[15] S. Shahbazpanahi, A. B. Gershman, Z. Q. Luo, and K. M. Wong, "Robust adaptive beamforming for general-rank signal model," *IEEE Trans. Signal Processing*, vol. 51, pp. 2257–2269, Sep. 2003.
[16] S. A. Vorobyov, A. B. Gershman, Z.-Q. Luo, and N. Ma, "Adaptive beamforming with joint robustness against mismatched signal steering vector and interference nonstationarity," *IEEE Signal Processing Lett.*, vol. 11, no. 2, pp. 108–111, Feb. 2004.
[17] R. Wu and Z. Bao, "Array pattern distortion and remedies in space-time adaptive processing for airborne radar," *IEEE Trans. Antennas Propag.*, vol. 46, no. 7, pp. 963–970, Jul. 1998.
[18] S. Durrani and M. E. Bialkowski, "Effect of mutual coupling on the interference rejection capabilities of linear and circular arrays in CDMA systems," *IEEE Trans. Antennas Propag.*, vol. 52, no. 4, pp. 1130–1134, Apr. 2004.
[19] H. Steyskal and J. S. Herd, "Mutual coupling compensation in small array antennas," *IEEE Trans. Antennas Propag.*, vol. 38, no. 12, pp. 1971–1975, Dec. 1990.
[20] S. J. Orfanidis, *Electromagnetic Waves and Antenna*. Piscataway, NJ: Rutgers Univ. Press, 2004.
[21] X. Zhengyuan, P. Liu, and X. Wang, "Blind multiuser detection: From MOE to subspace methods," *IEEE Trans. Signal Process.*, vol. 52, no. 2, pp. 510–524, Feb. 2004.
[22] M. H. Er, "Linear antenna array pattern synthesis with prescribed broad nulls," *IEEE Trans. Antennas Propag.*, vol. 38, no. 9, pp. 1496–1498, Sep. 1990.
[23] B. Widrow and J. McCool, "Comparison of adaptive algorithms based on the methods of steepest descent and random search," *IEEE Trans. Antennas Propag.*, vol. 24, no. 5, pp. 615–637, Sep. 1976.
[24] S. Choi and D. Yun, "Design of adaptive array antenna for tracking the source of maximum power and its application to CDMA mobile communication," *IEEE Trans. Antennas Propag.*, vol. 45, no. 9, pp. 1393–1404, Sep. 1997.
[25] P. S. Chang and A. N. Willson Jr., "Analysis of conjugate gradient algorithms for adaptive filtering," *IEEE Trans. Signal Processing.*, vol. 48, pp. 409–418, Feb. 2000.
[26] S. Attallah and K. Abed-Meraim, "Fast algorithms for subspace tracking," *IEEE Signal Processing Lett.*, vol. 8, pp. 203–206, 2001.
[27] M. H. Er and A. Cantoni, "A unified approach to the design of robust narrow-band antenna array processors," *IEEE Trans. Antennas Propag.*, vol. 38, no. 1, pp. 17–23, Jan. 1990.
[28] A. B. Bershman, G. V. Serebryakov, and J. F. Bohme, "Constrained Hung-Turner adaptive beam-forming algorithm with additional robustness to wideband and moving jammers," *IEEE Trans. Antennas Propag.*, vol. 44, no. 3, pp. 361–367, Mar. 1996.
[29] M. Agrawal and S. Prasad, "Robust adaptive beamforming for wideband moving, and coherent jammers via uniform linear arrays," *IEEE Trans. Antennas Propag.*, vol. 47, no. 8, pp. 1267–1275, Aug. 1999.
[30] V. Katkovnik and A. Gershman, "Performance study of the local polynomial approximation based beamforming in the presence of moving sources," *IEEE Trans. Antennas Propag.*, vol. 50, no. 8, Aug. 2002.

Ayman Elnashar was born in Egypt in 1972. He received the B.S. degree in electrical engineering from Alexandria University, Egypt in 1995 and the M.Sc. and Ph.D. degrees in electrical communications engineering from Mansoura University, Mansoura, Egypt, in 1999 and 2005, respectively.

From March 1997 to March 1998, he was an RF Design Engineer with Systel (Motorola Egypt). From March 1998 to February 2000, he was an RF Systems Engineer with the Wireless Laboratory of Egypt Electrical Authority (EEA), Mansoura, Egypt. From March 2000 to June 2005, he was with the Egyptian Company for Mobile Services (Mobinil), Cairo, Egypt. Currently, he is with the Department of Mobile Network Development (MND), Etihad Etisalat (mobily), Riyadh, Saudi Arabia, where he is responsible for BSS/UTRAN design and implementation in central region from mobily network. He has been engaged in the design, planning, and implementation of mobily UMTS/HSDPA network. His research interests include digital signal processing for wireless communications, DS/CDMA, multiuser detection, smart antenna, array processing, space-time processing, beamforming, robust adaptive detection and neural network.

Dr. Elnashar has been a Technical Reviewer for the IEEE TRANSACTIONS ON VEHICULAR TECHNOLOGY and EURASIP *Journal on Applied Signal Processing*.

Said M. Elnoubi was born in Alexandria, Egypt, in September 1951. He received the B.S. and M.S. degrees from Alexandria University, Alexandria, in 1974 and 1977, respectively, and the Ph.D. degree from Southern Methodist University, Dallas, TX, in 1980, all in electrical engineering.

From October 1974 to December 1977, he was an Instructor at Alexandria University. From January 1978 to December 1980, he was a Research Assistant at Southern Methodist University where, from January 1981 to August 1981, he was a Postdoctoral Fellow. From September 1981 to August 1987, he was an Assistant Professor of electrical engineering at the University of Illinois at Chicago. From September 1987 to June 1989, he was an Associate Professor in the Electrical Engineering Department, Alexandria University. From August 1989 to May 1990, he was a Visiting Professor at Wichita State University. From 1990 to 1994, he was a member of Technical Staff at MITRE Corporation, McLean, VA. Currently, he is a Professor in the Electrical Engineering Department, Alexandria University. His research interests include digital modulation, mobile radio and wireless communications, spread spectrum and air/ground radio communications.

Dr. Elnoubi received the Egypt National Incentive Award for Engineering Science and the Salah Amer Incentive Award for Electronic Science in 1989. He received the Egypt National Superiority Award for Engineering Science in 2003 and Alexandria University Distinction Award for Engineering Science in 2004. He has been a Technical Reviewer of the IEEE TRANSACTIONS ON COMMUNICATIONS, AEROSPACE AND ELECTRONIC SYSTEMS, VEHICULAR TECHNOLOGY, INFORMATION THEORY and *IEE Proceedings*. He was an Assistant Editor of *Communications* and the IEEE TRANSACTIONS ON VEHICULAR TECHNOLOGY. He is listed in *Marquis Who's Who in Science and Engineering*.

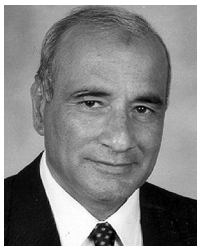

Hamdi A. El-Mikati (M'85–SM'96) received the B.Sc. and M.Sc. degrees in electrical engineering from Alexandria University, Alexandria, Egypt, in 1964 and 1969, respectively, and the Ph.D. degree from the Polytechnic Institute, Leningrad, U.S.S.R., in 1974.

Since 1975, he has been with the Faculty of Engineering, Mansoura University, Mansoura, Egypt, where he is currently a Professor of microwave communications. He was Head of the Department of Electronic Engineering from 1989 to 1992, Vice-Dean of the Faculty of Engineering from 1994 until 1998, and Dean of the Faculty from 1998 to 2003. His current interests include antenna arrays for wireless communications, microstrip antenna arrays, and computational electromagnetics.

Dr. El-Mikati is a member of the OSA and the National Radio Science Committee.